European Journal of Pharmaceutics and Biopharmaceutics 158 (2021) 233–244

Contents lists available at ScienceDirect

European Journal of Pharmaceutics and Biopharmaceutics

journal homepage: www.elsevier.com/locate/ejpb

Biological evaluation of new TEM1 targeting recombinant antibodies for radioimmunotherapy: *In vitro*, *in vivo* and *in silico* studies

Alice D'Onofrio [a], Lurdes Gano [a,b], Rita Melo [a], Filipa Mendes [a,b], Maria Cristina Oliveira [a,b], Thibaut Denoël [c], Niklaus Schaefer [c], David Viertl [c], Julie Fierle [d], George Coukos [e], Steven Dunn [d], John O. Prior [c], António Paulo [a,b,*]

[a] C^2TN- Centro de Ciências e Tecnologias Nucleares, Instituto Superior Técnico, Universidade de Lisboa, Portugal
[b] DECN - Departamento de Engenharia e Ciências Nucleares, Instituto Superior Técnico, Universidade de Lisboa, Portugal
[c] Department of Nuclear Medicine and Molecular Imaging, Lausanne University Hospital and University of Lausanne, Lausanne, Switzerland
[d] LAbCore, Ludwig Institute for Cancer Research, Lausanne University Hospital and University of Lausanne, Lausanne, Switzerland
[e] Ludwig Institute for Cancer Research and Department of Oncology, Lausanne University Hospital and University of Lausanne, Lausanne, Switzerland

ARTICLE INFO

Keywords:
TEM1
Radioimmunotherapy
Theranostics
Radioiodine
Antibody fragments

ABSTRACT

The tumour endothelial marker 1 (TEM1/endosialin/CD248) is a receptor overexpressed in several human solid tumours and silenced in normal adult tissues, representing a suitable and potentially safe target for radioimmunotherapy of sarcoma. To develop new tools with improved TEM1 targeting properties, a new panel of antibody fragments was for the first time evaluated preclinically following ^{125}I radiolabelling. The antibody fragment 1C1m-Fc, with the highest human/murine TEM1 binding affinity, was extensively characterized *in vitro* and *in vivo* in a Ewing's sarcoma human xenograft mouse model. *In silico* studies were also performed to elucidate the influence of a single amino acid mutation in the complementarity-determining region (CDR3) of the heavy chain, upon affinity maturation of the parental clone 1C1-Fc. From this study, 1C1m-Fc emerged as a promising candidate for the development of TEM1-targeted radioimmunoconjugates, namely to be further explored for theranostic applications with other suitable medical radionuclides.

1. Introduction

Research in the field of Radioimmunotherapy (RIT) has been intensive in the last 50 years as the unique synergy between the highly specific antibody-antigen interaction and the selective delivery of radiotoxicity to tumour cells has yielded significant successes in oncological applications [1–3]. Therapy with radioimmunoconjugates is highly relevant in haematological malignancies, such as lymphomas and leukaemia, as these cancers are more sensitive to ionizing radiation and more easily accessible than solid tumours and their complex microenvironment [4–7]. Several strategies have been reported to increase the efficacy of RIT against solid tumours such as the combination with other therapies, intra-compartmental injections and pre-targeting approaches through the use of bi-specific antibodies or click-chemistry [8,9]. Additionally, smaller antibody fragments derived from monoclonal antibodies or produced recombinantly are currently available to overcome some of the limitations associated with the use of full-length monoclonal antibodies, bringing advantages such as reduced cost and easiness of production, improved pharmacokinetics, higher stability to low pH, and the capacity to penetrate deeper in tissues or in tumours [10,11].

The endosialin/CD248/TEM1 is an appealing and promising biological target still poorly explored in cancer therapy. TEM1 is a type I cell surface glycoprotein of 757 amino acids structurally related to thrombomodulin [12–15]. TEM1 expression is negligible in adult blood vessels however in several carcinomas TEM1 overexpression has been found in endothelial cells, pericytes and tumour-associated fibroblasts, indicating a role in vascular cell adhesion and migration, neoangiogenesis, tumour progression and metastatization [16–21]. A study conducted with TEM1 knock-out mice indicated that the absence of this protein did not affect overall health and normal wound healing. Nevertheless, after transplantation of tumours to abdominal sites, a striking reduction in tumour growth, invasiveness, and metastatization was reported, highlighting the important functional role of TEM1 in tumour progression [22]. In sarcomas, a class of heterogeneous cancers originating from cells of

* Corresponding author at: C2TN- Centro de Ciências e Tecnologias Nucleares, Instituto Superior Técnico, Universidade de Lisboa, Portugal.
E-mail address: apaulo@ctn.tecnico.ulisboa.pt (A. Paulo).

https://doi.org/10.1016/j.ejpb.2020.11.015
Received 27 June 2020; Received in revised form 17 November 2020; Accepted 23 November 2020
Available online 30 November 2020

connective tissue or bone, TEM1 expression has been found not only in tumour vessels and in the stromal compartment, but also on the malignant cells themselves. In a study analysing over 203 clinical sarcoma specimens from 19 types of sarcoma subtypes, 96% of the collected samples stained positively for TEM1 and, in 77% of tumours, TEM1 expression was found both on vascular and tumour cells [23]. Due to this favourable expression pattern, antibody-mediated therapy targeting TEM1 holds great potential for the treatment of sarcoma.

A humanized monoclonal antibody (MORAb-004) targeting TEM1 was developed and received FDA orphan drug designation for sarcoma after undergoing Phase I and Phase II clinical trials in patients [24,25]. MORAb-004 was obtained by immunizing mice with human fetal fibroblasts. Humanization was achieved by grafting of the six complementarity determining regions (CDRs) on a human IgG1κ framework. One of the major limitations of MORAb-004 is the lack of murine TEM1 cross-reactivity, requiring the use of engineered cell lines and mouse models featuring huTEM1-positive grafts for its pre-clinical evaluation [26].

A TEM1-specific fully-human antibody fragment (scFv78), with high affinity for human and murine TEM1, was successively developed and fused to an immunoglobulin Fc domain, to obtain a dimeric molecule with improved avidity, stability and pharmacokinetics for *in vivo* optical imaging [16]. The antibody fragment scFv78-Fc retained high target affinity upon both ^{125}I-radiolabelling and conjugation with a near-infrared (NIR) probe. Biodistribution studies and NIR imaging studies in different TEM1-expressing mouse models, demonstrated negligible uptake in critical tissues such as heart, lung, kidney, liver and brain, while revealing high accumulation in both human and murine TEM1 positive lesions [27]. The same antibody fragment scFv78-Fc was recently evaluated in RD-ES Ewing's sarcoma and SK-N-AS neuroblastoma tumour mice models, following ^{111}In radiolabelling. Biodistribution studies confirmed tumour targeting in both models and the extrapolated human dosimetry was found to be in the range of other diagnostic ^{111}In radiolabelled monoclonal antibodies in clinical use [28]. Another study from the same group used the unconventional positron emitter ^{152}Tb to assess the feasibility of microPET-based dosimetry in a Ewing's sarcoma tumour mouse model. The results obtained by PET/CT, compared to the classic biodistribution experiments, resulted in overall acceptable dose discrepancies [29].

In this work, a panel of novel fully human scFv-Fc antibody fragments targeting the TEM1 receptor, produced according to a recently published procedure, were radiolabelled for the first time with ^{125}I [30]. The direct radioiodination of the antibody fragments *via* tyrosine residues allowed their *in vitro* and *in vivo* biological evaluation in human and murine cellular models [31–33]. The influence of the radiolabelling method on the TEM1 binding was analysed by comparison of the *in vitro* biological performance of the radiolabelled scFv-Fc obtained by a direct and indirect radioiodination approaches. The best performing antibody, showing the highest hu/mu TEM1 affinity, was extensively evaluated and comprehensively characterized *in vitro* before performing a preliminary *in vivo* biodistribution experiment using a Ewing's sarcoma mouse model.

Interestingly, the most promising molecule was developed by affinity maturation of the antibody scoring the lowest affinity in the same assay, upon a single amino acid substitution at residue 233. This residue is located in the complementarity-determining region (CDR3) of the heavy chain and seems to play an important role in TEM1 binding, as indicated by the results from the experimental assays. Encouraged by these findings, we performed several *in silico* experiments to further explore the influence of this residue and to elucidate its role in the improved binding of the antibody to both the murine and human TEM1 orthologs.

2. Results

2.1. Radiolabelling and stability studies

A panel of five scFv antibody fragments, selected by Phage Display for their huTEM1 affinity, were reformatted as scFv-Fc fragments to develop new potential TEM1 radiommunoconjugates. These scFv-Fc fragments (1C1-Fc, 4D8-Fc, 3F4-Fc, 3B6-Fc and 1C1m-Fc) were radiolabelled on the tyrosine residues with ^{125}I, according to the Iodogen method [34]. The radioiodinated antibodies were obtained with specific activities between 4 and 72 MBq/nmol and an average radiochemical yield above 90%. All ^{125}I-labelled antibody fragments presented a very high radiochemical purity of 99%, as determined by ITLC (Instant Thin Layer Chromatography) analysis following purification by ultrafiltration (see Supporting Figure S1). Possible effects of the radioiodination on the antibody structure were further verified by size-exclusion (SE) HPLC and SDS-PAGE analyses of the antibodies before and after radiolabelling. Both analysis confirmed preserved structural integrity of the molecules after the radiolabelling procedure (see Figure S2 and S3 in SI).

The radiochemical stability of the radioiodinated antibodies was evaluated by ITLC analysis after incubation for 48 h at 37 °C and 4 °C in both Phosphate-Buffered Saline (PBS) pH 7.2, and cell culture medium (Dulbecco's Modified Eagle Medium, DMEM). In PBS the radioiodinated antibodies exhibited high *in vitro* stability, retaining radiochemical purity values above 90% after the incubation period, with the exception of the 1C1-Fc clone, which showed a lower radiochemical purity of 80% at both temperatures. In cell culture media, all molecules showed radiochemical purity above 90% after 48 h of incubation at both temperatures (see Fig. S4 in SI).

The radioiodination of the antibody fragment 1C1m-Fc, selected as the most promising in the *in vitro* evaluation, was also performed through acylation of lysine residues using the ^{125}I-labelled Bolton-Hunter reagent [35]. This approach, however, yielded radiolabelled antibodies with lower specific activities (18–90 MBq/mg) than those obtained by the direct radioiodination, with an average radiochemical yield of 20% and a radiochemical purity of 99%, as determined through ITLC analysis following purification by ultrafiltration (see Fig. S5 in SI).

2.2. Evaluation in cellular models

The panel of five TEM1-targeting recombinant antibodies was screened in several cell lines to identify the most promising candidate for radioimmunotherapy. The murine 2H11 cell line, previously reported as a good model for tumour endothelium, was chosen for its well characterized high surface expression of muTEM1 [33]. The A673 cell line, established from a patient with a primary Ewing's sarcoma and reported as a useful model for the study of endosialin-directed therapies, was chosen for its moderate cell surface huTEM1 expression. As a negative control, the endothelial murine cell-line MS1, with no reported TEM1 expression, was used [27,32,33].

2.3. Selection of the best performing clones: studies in TEM1$^+$ and TEM1$^-$ murine cells

Uptake studies were performed with the radiolabelled antibody fragments, and 3F4-Fc and 1C1m-Fc were identified as the two clones with the highest uptake in the muTEM1$^+$ cell line (Fig. 1), reaching maximum uptake values (per million cells) of 14% and 36%, respectively, after 24 h of incubation. The other three clones 4D8-Fc, 1C1-Fc and 3B6-Fc had a very low uptake and were therefore not considered in the following studies. None of the antibodies was observed to be taken up significantly by the MS1 cells (below 3%, data not shown), suggesting a selective TEM1-mediated uptake.

The internalization rate after the formation of the antibody-antigen complex is a crucial parameter when assessing the biological potential of a new antibody [36,37]. An internalization assay was performed for the two radioiodinated antibodies that presented the highest uptake values, 3F4-Fc and 1C1m-Fc, using the muTEM1+ cell line 2H11. At the selected time points, the surface-bound and internalized antibody fractions were recovered separately and counted. The two antibodies showed initially a similar rate of internalization, with 16% and 12% for

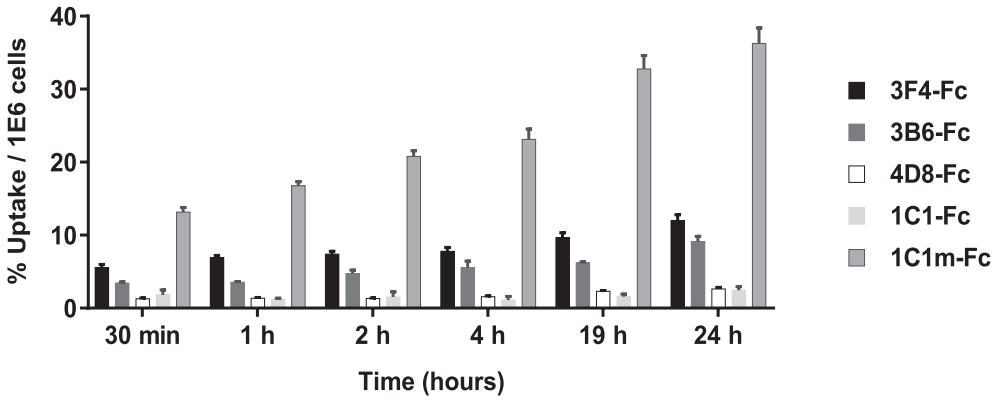

Fig. 1. Cellular uptake values in the 2H11 (muTEM1$^+$) cell line of the ^{125}I-radiolabelled 3F4-Fc (n = 5), 3B6-Fc (n = 2), 4D8-Fc (n = 2), 1C1-Fc (n = 2), 1C1m-Fc (n = 3).

3B4-Fc and 1C1m-Fc, respectively, of the total activity bound to the cell internalized after 30 min, as shown in Fig. 2. This value increased slowly over time for the fragment 3F4-Fc, with 32% of the total cell-associated activity internalized. For the fragment 1C1m-Fc, the internalization presented a higher increase overtime and reached, after 24 h of incubation, 44% of the total bound activity.

The two clones 3F4-Fc and 1C1m-Fc were further investigated in a saturation assay, which was performed with the radioiodinated antibodies to determine their binding affinity and the receptor density in the murine cell line 2H11. These parameters, expressed by the K_d and B_{max}, were calculated from a non-linear regression fit of the specific binding data (Fig. 3). The K_d values obtained were encouragingly in the low nanomolar range and very similar for the two clones, with values of 4.7 ± 1.2 nM and 5.2 ± 2 nM for 3F4-Fc and 1C1m-Fc, respectively.

These K_d values appear to be comparable to those previously reported in the literature for similar radioiodinated TEM1 targeting molecules. As an example, the K_d value determined for ^{125}I-78Fc in a similar assay, using the engineered cell line MS1-TEM1, was 0.95 ± 0.05 nM [27]. The TEM receptor density in the 2H11 cell line, expressed as B_{max}, was determined to be 1.4 × 10^5 binding sites/cell in both experiments, confirming the high TEM1 expression of this murine cell line chosen for the *in vitro* muTEM1 model.

2.4. Evaluation of the best performing clones in human tumoural cells

The radiolabelled 3F4-Fc and 1C1m-Fc clones were next evaluated for their binding to the human TEM1 receptor. The assays were carried out using the A673 cell line of human origin derived from Ewing's sarcoma and characterized by a moderate TEM1 expression.

The 3F4-Fc antibody fragment showed only a modest affinity for the human TEM1 receptor reflected by a maximum uptake value of 4% in the A673 cells, after 24 h. However, the 1C1m-Fc clone showed an encouraging uptake in this cell line, with a maximum value of 23% after 24 h, suggesting a good binding affinity also for huTEM1, as shown in Fig. 4 a.

The cellular uptake results allowed us to identify the 1C1m-Fc fragment as the most promising candidate. Therefore, our subsequent investigations focused only on this antibody fragment and included blocking and saturation assays, as well as internalization studies. The blocking assays, shown in Fig. 4 b, were performed on both muTEM1$^+$ and huTEM1$^+$ cell lines, by incubating the cells with the ^{125}I-1C1m-Fc antibody in the presence and absence of an excess of cold 1C1m-Fc. The results highlighted how, in the presence of the cold antibody, a complete blocking of the uptake was induced, indicating a specific TEM1-mediated mechanism in both human and murine cell lines.

The rate of internalization of the radioiodinated 1C1m-Fc was also determined in the huTEM1 expressing cell line A673. The assay was performed over 24 h, similarly to the previous internalization assay, and is shown in Fig. 5. After 30 min, the internalization was around 16% of the total cell-associated activity and did not significantly increase during the following 4 h. However, similarly to the previous assay, at the longer incubation time points of 19 and of 24 h, half (53%) of the cell associated activity was internalized.

The saturation assay data for the A673 cell line, presented in Fig. 6, allowed the quantification of the binding affinity of the radioiodinated 1C1m-Fc antibody for the human TEM1 ortholog and the assessment of receptor density in this cell line. A K_d value of 0.9 ± 0.5 nM was determined in the A673 line, which is five-times lower than the K_d obtained in the muTEM1$^+$ cell line, but in accordance with the K_d determined for a similar radioiodinated molecule using an engineered TEM1

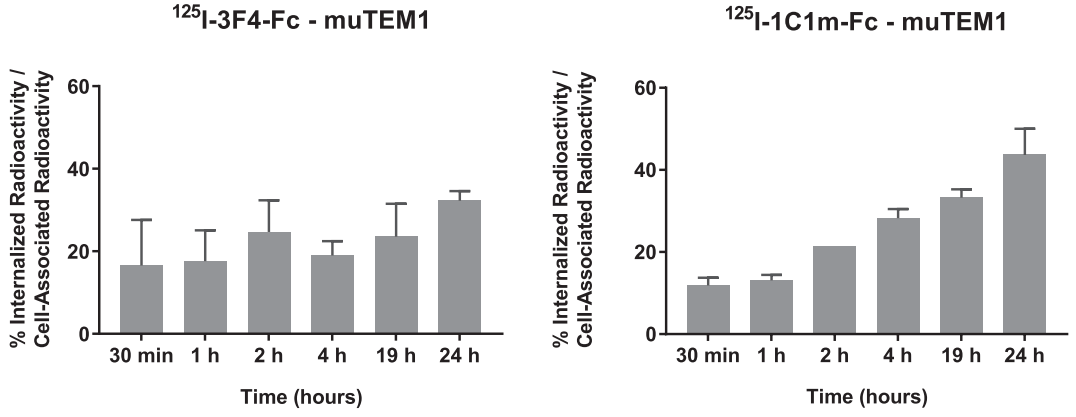

Fig. 2. ^{125}I-3F4-Fc (n = 2) and ^{125}I-1C1m-Fc (n = 1) internalization results in 2H11 cell line.

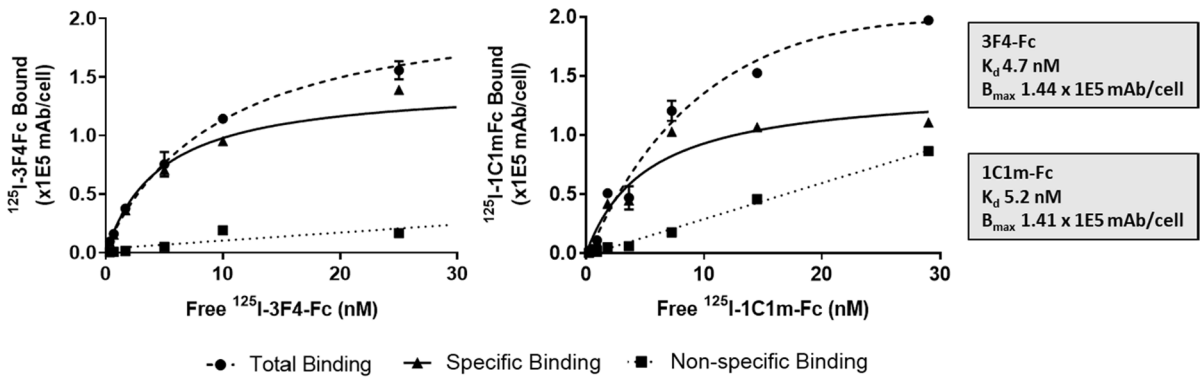

Fig. 3. Saturation assays of radioiodinated 3F4-Fc (n = 1) and 1C1m-Fc (n = 1) antibodies in 2H11 cell line (K_d values expressed in nM and B_{max} values expressed as binding sites per cell).

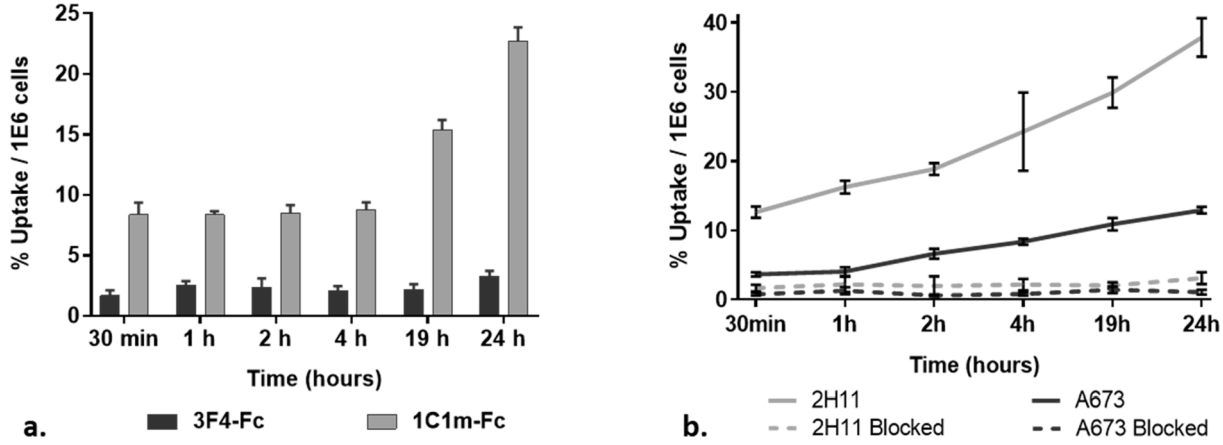

Fig. 4. a. Cellular uptake values for the ^{125}I-3F4-Fc (n = 2) and ^{125}I-1C1m-Fc (n = 3) in A673 (huTEM1$^+$) cell lines. **b.** Blocking assay of ^{125}I-1C1m-Fc (n = 1) on 2H11 (muTEM1) and A673 (huTEM1).

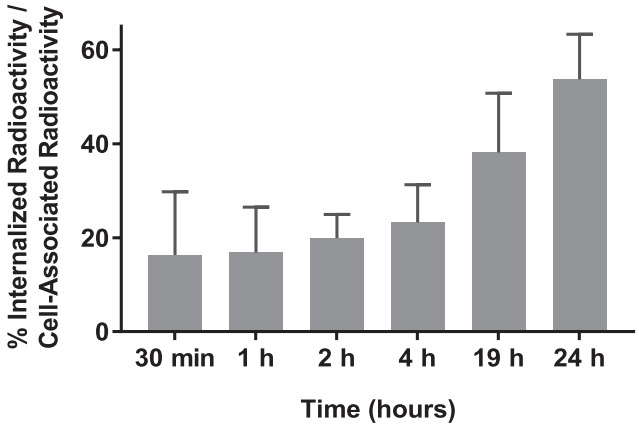

Fig. 5. ^{125}I-1C1m-Fc internalization assay in A673 (huTEM1$^+$) cell line.

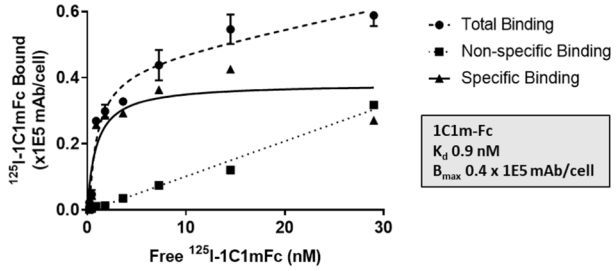

Fig. 6. Saturation assay of ^{125}I-1C1m-Fc antibody in A673 cell line (K_d values expressed in nM and B_{max} values expressed as binding sites per cell).

expressing cell line, as mentioned above [27]. This result suggests a higher affinity of the 1C1m-Fc antibody for the huTEM1 receptor. However, in agreement with the lower TEM1 expression of this cell line, the receptor density expressed by the B_{max} value is four-times lower (0.4×10^5 binding sites/cell), which can explain the lower uptake values found using the human cell line compared to the murine cell line (see Fig. 4) [31,33].

To gain a further insight on the binding ability of the ^{125}I-1C1m-Fc fragment towards the huTEM1 receptor, we next proceeded with the determination of its immunoreactive fraction (IRF) using the human TEM1 protein and following a recently published method based on a rectangular hyperbolic fit of the experimental data [38]. The study was conducted for an antibody fragment concentration of 0.18 nM and the obtained results led to a calculated IRF value of 82%, as shown in Fig. 7.

Despite the favourable results obtained with the ^{125}I-1C1m-Fc directly labelled through the incorporation of radioiodine in tyrosine residues, it was considered that such a labelling strategy could potentially interfere with the interaction of the clone with the TEM1 receptor, due to the presence of tyrosine residues in the antigen binding site. To investigate this issue, the cellular uptake of ^{125}I-1C1m-Fc radioiodinated directly on the tyrosine residues or indirectly through the acylation of the lysine residues with the radioiodinated Bolton-Hunter (BH) reagent was compared. The studies were conducted using both the 2H11 and A673 cell lines and comprised also antigen blocking experiments.

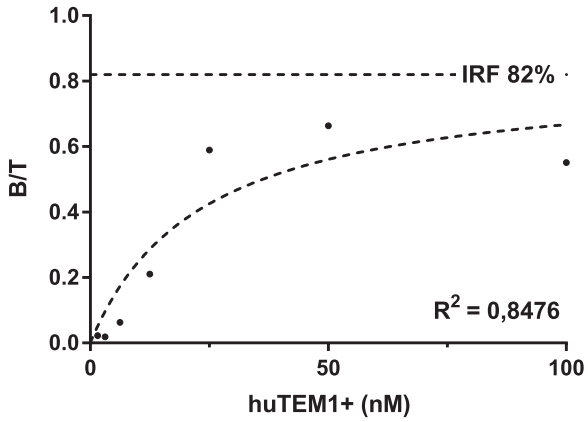

Fig. 7. Immunoreactive fraction assay for the ^{125}I-1C1m-Fc antibody at a concentration of 0.18 nM (the goodness of fit, expressed by R^2, was determined to be 0.8476).

The results obtained, displayed in Fig. 8 b, revealed a significant enhancement of the uptake values observed in the murine cell line 2H11 for the antibody radiolabelled using the Bolton-Hunter procedure. Nonetheless, the increase observed in the human cell line was modest and allowed us to conclude that, at least in the A673 cell line, the radioiodination using the Iodogen method did not significantly compromise the binding affinity of the antibody for the TEM1 target receptor. (P values greater than 0.01, multiple T-tests).

2.5. Evaluation in a Ewing's sarcoma mouse model

A biodistribution study was performed with ^{125}I-1C1m-Fc in nude mice bearing A673 xenografts in a Ewing's Sarcoma mice model. The results of the biodistribution, shown in Fig. 9, indicate a relatively rapid tumoural uptake, with 4% of the injected dose per gram (% ID/g) at 4 h post-injection (p.i) and a maximum uptake of 5% ID/g occurring at 24 h. The values were persistent until 72 h p.i., indicating a high tumoural retention.

Non-target uptake was mostly observed in the liver, spleen and kidneys. The activity found in the liver, due to the metabolism of radiolabelled antibodies, decreased overtime and at 24 h p.i. was below 5% ID/g. The highest uptake value of 35% ID/g was found at 4 h p.i. in the spleen. This high spleen uptake decreased to below 10% ID/g at 48 h and is consistent with the *in vivo* behaviour of a previously reported unrelated TEM1-targeting scFv-Fc [27,28]. The uptake in the kidneys at 4 h p.i. was 18% ID/g, with the value decreasing constantly over time until reaching 6% ID/g at 72 h. The activity in the blood decreased from 11% ID/g at 4 h p.i. to 2% ID/g after 72 h indicating a slow blood clearance as expected for Fc-containing antibody constructs of this molecular weight (130 kDa).

The tumour/blood ratio was seen to increase over time from 0.3 at 4 h p.i. to a maximum value of 1.8, reached at 72 h. The tumour to muscle ratio doubled between 4 and 24 h p.i. and then remained constant through the following 72 h. The administration of KI and $KClO_4$, to block the thyroid and prevent uptake of ^{125}I after *in vivo* dehalogenation, was efficient in reducing the values to below 5% ID/g. A significant level of uptake and retention was observed in the ovaries in accordance with what has been seen in other studies, suggesting that healthy ovarian and uterine tissues might have a non-negligible TEM1 expression [26,27,39].

2.6. Impact of mutating threonine to leucine at position 233

The antibody fragment 1C1m-Fc that emerged from this pre-clinical study as the most promising candidate for TEM1 radioimmunotherapy was produced by affinity maturation of its parental, huTEM1-specific scFv clone, 1C1 (alternative ID: HS06), as recently published [30]. Screening for a molecular variant with increased binding affinity and hu/muTEM1 cross-reactivity resulted in the isolation of the improved scFv variant, 1C1m (**m**utant), and the construction of 1C1m-Fc. The improved binding performance of 1C1m required only the replacement of a single VH CDR3 threonine (residue 233) by a leucine. Despite this single point mutation, a striking difference in the binding affinity for muTEM1 was observed between 1C1-Fc and 1C1m-Fc, as indicated by their respective rates of uptake in muTEM1$^+$ 2H11 cells (see Fig. 1). To better characterize this difference between the two proteins, we decided to carry out comparative *in vitro* assays with radioiodinated 1C1-Fc and 1C1m-Fc in murine and human TEM1 expressing cell lines. For a more robust comparison of the results between the cell lines, these cellular uptake assays were performed using the same batches of radioiodinated antibodies, under the same experimental conditions.

As expected, and shown in Fig. 10, both molecules were taken up by human A673 cells. However, ^{125}I-1C1m-Fc exhibited significantly higher uptake levels than those exhibited by the parental antibody ^{125}I-1C1-Fc in the human cell line, confirming the improved affinity of the mutant clone for the huTEM1 receptor. Nonetheless, this difference in the uptake values in human cells was decisively less pronounced than the one in the muTEM1$^+$ cells, with these data confirming the huTEM1 selectivity of the 1C1-Fc parent clone.

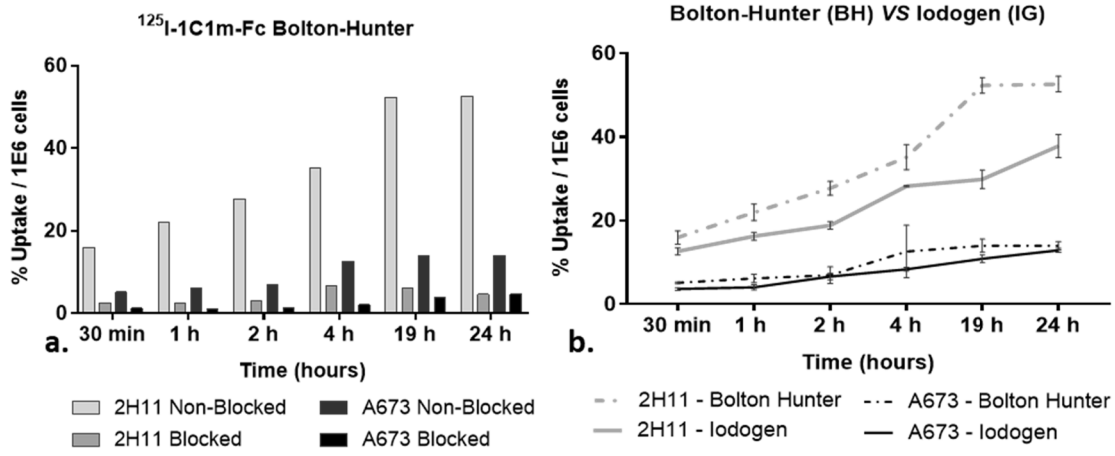

Fig. 8. a. Blocking results of ^{125}I-1C1m radiolabelled by BH method in 2H11 (grey) and A673 (black) cell lines. **b.** Comparison with ^{125}I-1C1m-Fc radiolabelled by the BH (dotted line) and IODOGEN method (straight line in 2H11 (grey) and A673 (black) cell lines).

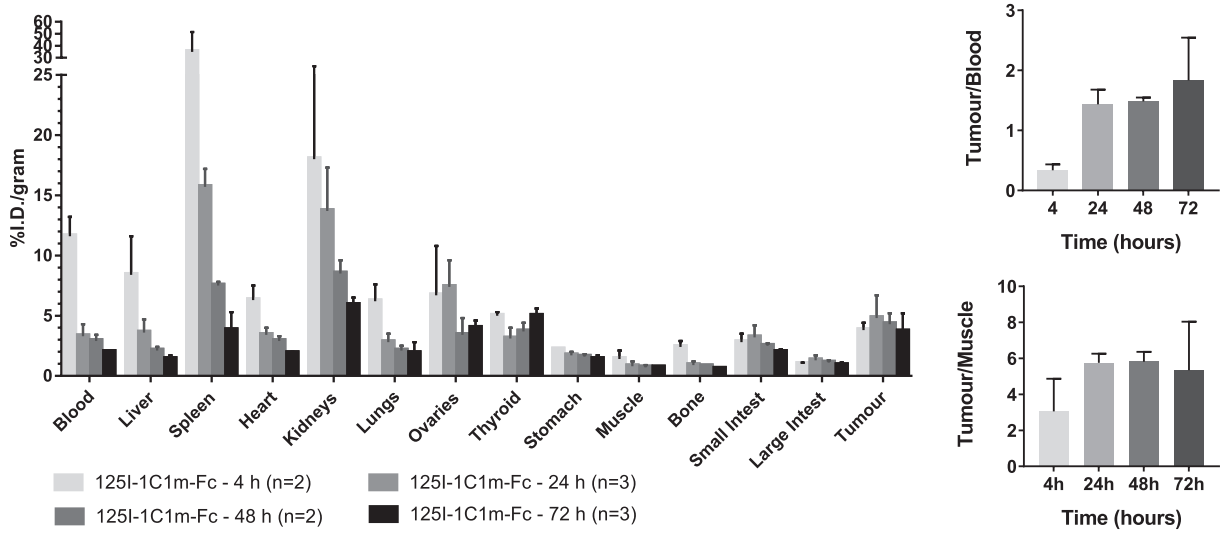

Fig. 9. Biodistribution data for ^{125}I-1C1m-Fc in A673 xenografts bearing mice, expressed as % I.D./g of organ, including the Tumour/Blood and Tumour/Muscle ratios (mean ± S.D., n = 2 for 4 h and 48 h or n = 3 for 24 h and 72 h).

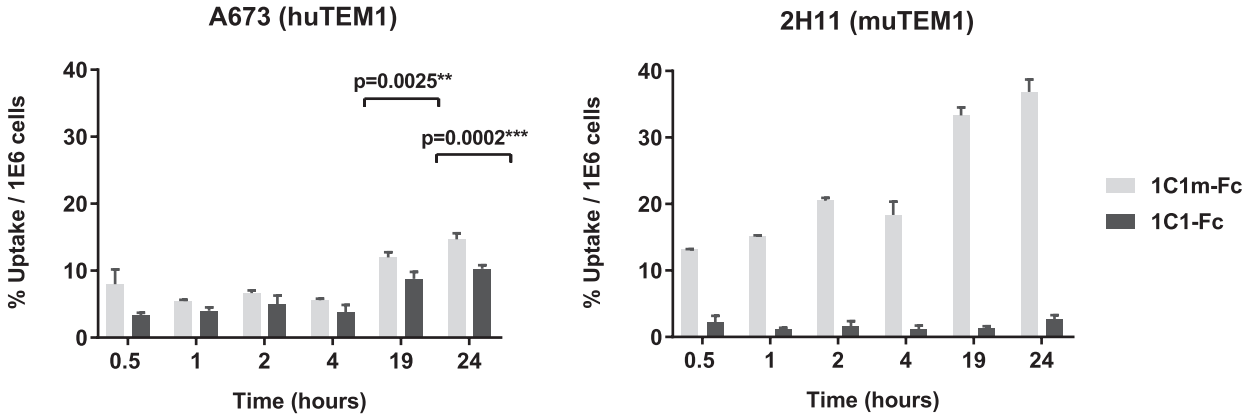

Fig. 10. Cellular uptake values for ^{125}I-1C1-Fc (n = 2) and ^{125}I-1C1m-Fc (n = 1) in A673 and 2H11 cell lines.

2.7. *In silico studies*

To explore further the influence of the the single amino acid substitution between 1C1-Fc and 1C1m-Fc, we performed molecular docking studies using a computer-guided homology modelling procedure. The 3D-structures of the conserved region of both murine and human TEM1 extracellular domains, described as the binding site of anti-TEM1 recombinant antibodies [40], were docked onto models of the 1C1-Fc and 1C1m-Fc antibody fragments, in order to assess the most stable structure of each complex. The HADDOCK webserver allows both side chains and the backbone to move at the refinement stage, increasing the accuracy of the scoring compared with classical rigid body docking. The comparison between the best docking models of the four complexes, based on their highest HADDOCK scores [41], revealed slight differences. In both systems (human and murine), the best scores were obtained with the 1C1m-Fc complexes versus the 1C1-Fc complexes: muTEM1/1C1m-Fc (-150.8) compared with muTEM1/1C1-Fc (-148.4), and huTEM1/1C1m-Fc (-122.3) compared with huTEM1/1C1-Fc (-113.2).

Furthermore, visual inspection of the predicted binding modes indicated that the best predicted complexes involved conformational changes within the binding sites. A conserved epitope was predicted by PyMOL (see Supporting Figure S6). The THR233ILE mutation clearly influences the antibody fragment binding site and induces interface changes. In particular, the predicted epitopes for 1C1m-Fc in huTEM1 and muTEM1 highlight that ILE233 seems to be a relevant residue at the interface, as opposed to huTEM1 and muTEM1 complexes with 1C1-Fc where THR233 is not considered a interfacial residue (see Supporting Figure S6).

Molecular dynamics (MD) simulations were used to analyse the differences in the global dynamics of the studied systems, using the most favourable docking structures as the initial conformations of the MD simulations. Three replicas of 100 ns were performed to explore the dynamic properties of the docked mu/huTEM1/1C1(m)-Fc complexes in water. Snapshots of MD simulations from the final structures shown in Fig. 11, indicate a clear influence of the THR233ILE mutation in the interface between the TEM1 and the antibodies, in both human and murine models. However, this influence is more evident in the muTEM1 complex system, as shown in Fig. 11 C and D.

The interface of the mu/huTEM1/1C1-Fc complexes was predicted using Pymol, with a cut-off distance of 5 Å between the C-alpha pair of the residues involved in protein-protein interactions. Considering the change of the interface over time, we were able to obtain a realistic picture of the dynamic behaviour of these systems. To quantify the influence of the mutation on the dynamic behaviour of TEM1/1C1(m)-Fc bindings, we used root mean square fluctuation (RMSF) calculations (see Figure S7 in SI). The residues involved in the interaction with 1C1m-Fc, for both huTEM1 and muTEM1, showed lower fluctuation amplitudes

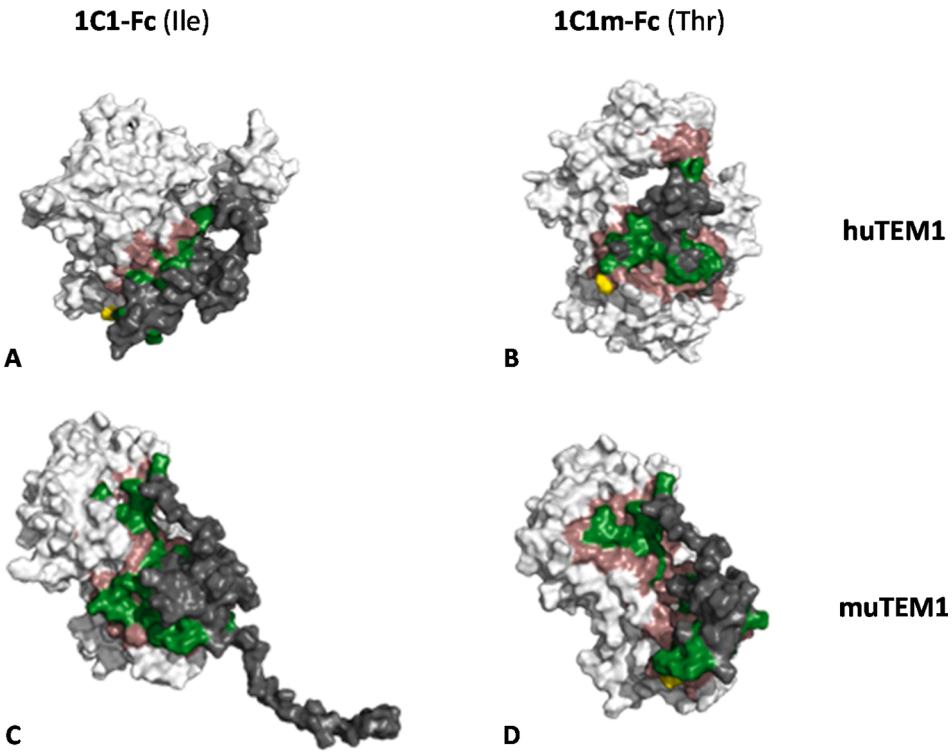

Fig. 11. Snapshots of molecular dynamics simulations from the final structures (100 ns). (**A**) huTEM1 (dark grey) complexed with 1C1-Fc (white); (**B**) huTEM1 (dark grey) complexed with 1C1m-Fc (white); (**C**) muTEM1 (rose) complexed with 1C1-Fc (green); (**D**) muTEM1 (rose) complexed with 1C1m-Fc (green). In all images, huTEM1 and 1C1-Fc interface is represented in dark rose and green, respectively. THR233 and ILE233 are represented in yellow at 1C1-Fc and 1C1m-Fc complexes. (For interpretation of the references to color in this figure legend, the reader is referred to the web version of this article.)

when compared to the residues of 1C1-Fc. Even if in the 250–270 region of the muTEM1/1C1m-Fc system a high fluctuation is observed (Fig. S7 D, SI), the average RMSF is still lower when compared to the other systems, since more residues are involved in the interface.

The average number of H-Bonds established between interfacial residues during the simulations were calculated as relevant information to explain how the THR233ILE mutation influences the binding with the target receptor. Our results indicated that the THR233ILE mutation positively influences the binding, with an increase in the total predicted number of H-bonds between the 1C1m-Fc antibody and both the human and murine TEM1. In particular, the complex muTEM1/1C1m-Fc scored the highest number of H-Bonds at interface as shown in Fig. 12.

3. Discussion

The membrane receptor TEM1 has emerged in the last years as an attractive biological target for anticancer therapies [17,23,27]. TEM1 expression has been found both in tumour stroma and neo-vasculature and its pivotal role in the processes of tumour progression and survival regulated by the tumour microenvironment has been demonstrated in several studies [28,29,12]. Additionally, the analysis of several sarcoma clinical specimens revealed TEM1 expression both on malignant cells and on tumour vessels. Therefore, TEM1 is considered as a promising target for antibody-mediated therapy of sarcomas. In fact, this approach would allow to combine synergistically a direct anticancer effect on the tumoural cells with a concomitant effect on the tumour microenvironment, hampering the eventual survival, proliferation and metastatization of residual tumour cells [23]. Currently, one TEM1 targeting antibody is being evaluated in several clinical trials [24,25]. Hence, the development of additional molecules with improved pharmacokinetic properties and alternative therapeutic strategies might prove advantageous in this regard, in addition to furthering our understanding of the potential of TEM1 targeted therapies.

Towards this goal, we decided to conduct an initial pre-clinical investigation of several members of a recently isolated panel of novel, fully human TEM1 targeting antibody fragments using ^{125}I radiolabelling. After optimization of the radioiodination, possible effects on the structural integrity of the radioiodinated molecules were evaluated

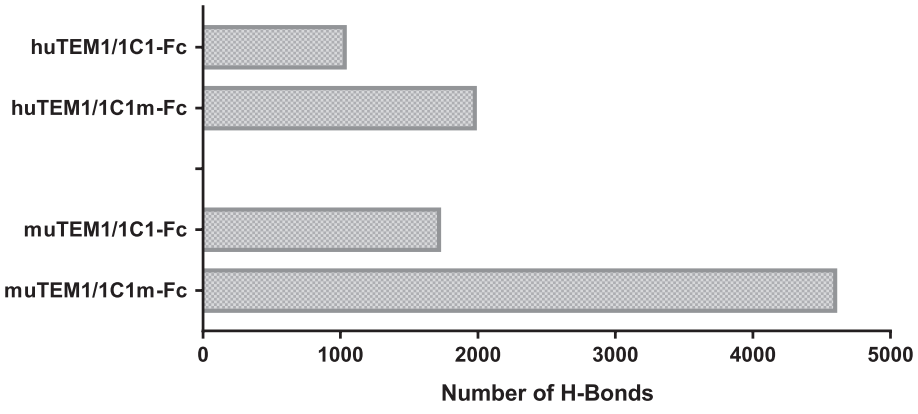

Fig. 12. Total number of H-Bonds in the interface, during molecular dynamics simulation time, for each of the four systems.

using complementary techniques, including size exclusion HPLC and SDS-Page. Their radiochemical stability was also evaluated in different media and temperatures, before continuing with their *in vitro* and *in vivo* functional characterization. The first round of studies on five tested molecules led to the identification of 1C1m-Fc as the antibody fragment with the highest binding affinity for the murine TEM1 receptor. The strong murine cross-reactivity of the 1C1m-Fc clone was considered an important advantage for conducting *in vivo* studies using human xenografts, such as the Ewings sarcoma tumour model used here, as the microenvironment responsible for the implantation and growth of the tumour cell lines will express the murine TEM1 receptor [42].

The immunoreactivity (expressed as the immunoreactive fraction) of the prepared ^{125}I-1C1m-Fc towards the human TEM1 receptor was assessed using a recently described procedure and determined to be greater than 80% [38]. Following the establishment of 1C1m-Fc as the principal clone of interest, an extensive *in vitro* evaluation of the 1C1m-Fc using TEM1^{+} human and murine cell lines, as well as a TEM1 null murine line, confirmed the specificity of the molecule, with negligible uptake observed for the latter cells, and potent blocking of uptake in the TEM1^{+} cells by unlabelled cold antibody. Furthermore, internalization data indicates that the rate of internalization of ^{125}I-1C1m-Fc is quite slow, both in human and murine cells with different TEM1 levels, with appreciable internalization requiring 24 h of incubation, suggesting that the antibody does not trigger the rapid migration of TEM1 from the cell surface. At this time, it is not known whether 1C1m-Fc can physically crosslink adjacent TEM1 molecules.

The analysis of the saturation assay allowed us to estimate K_d and B_{max} metrics for both murine and human cell lines. The results indicated a low nM binding affinity of the selected antibodies towards the target receptor, with K_d values in the range reported for previously characterised anti-TEM1 antibody fragments [27]. Interestingly, the results obtained suggest a higher binding affinity of the ^{125}I-1C1m-Fc for the huTEM1 receptor, despite the higher uptake measured in the assay with the murine cell line. This behaviour could be explained by the known overexpression of TEM1 in the murine 2H11 cell line and is consistent with the higher B_{max} value determined for these cells relative to the human A673 line (1.4 versus 0.4 $\times$ 10^5 binding sites/cell, respectively). A contribution due to a greater avidity-driven/rebinding component mediated by the bivalent antibody towards the higher target density on the 2H11 cells also cannot be excluded.

The amino acid sequence of 1C1m-Fc has tyrosine residues located within the antigen binding CDR3 loop of the heavy chain [30]. The radioiodination of these residues could potentially induce a loss in the binding affinity of the resulting radiolabelled molecule when compared with the original antibody. By comparing two distinct radioiodination approaches targeting both tyrosine and non-tyrosine residues, we addressed this risk and, in the case of 1C1m-Fc, confirmed that direct iodination *via* tyrosine and indirect labelling *via* general lysine chemistry are both well-tolerated. These observations provide important insights with regard to future perspectives for developing 1C1m-Fc for both imaging and therapeutic applications. For example, unlike ^{131}I, which has seen extensive use in the clinic for both imaging and therapy, many of the matched radioisotope pairs suitable for theranostic applications are radiometals, such as ^{68}Ga/^{177}Lu. In this case, the conjugation of a suitable radiometal chelator to the carrier antibody is often achieved through the acylation of free lysine side-chain amino groups and our data would suggest that 1C1m-Fc may be compatible with such a labelling approach. The radioiodinated 1C1m-Fc antibody was further evaluated in a Ewing's sarcoma xenograft mouse model. The outcome of our biodistribution study demonstrated an *in vivo* behaviour comparable to that of other TEM1 targeting molecules with similar structures [23,27–29].

The discrepancy observed in the biological performance of the two antibodies 1C1m-Fc and its parent 1C1-Fc, is due to a single amino acid substitution at residue 233. This missense mutation was isolated following random error-prone mutagenesis of the entire 1C1 scFv and stringent phage display affinity screening against both human and murine TEM1. The present work confirms the improved binding affinity of 1C1m-Fc towards huTEM1, and the acquisition of strong muTEM1 cross-reactivity (which is absent in the 1C1-Fc parent clone). To further investigate the influence of the point mutation in these experimental results, we have performed *in silico* studies, namely to elucidate how such mutation influences the antibody-antigen interactions. The results of the docking studies revealed different conformational rearrangements with the THR233ILE mutation leading to different putative binding sites. Snapshots of MD simulations corroborated that the antibody-receptor interface varies depending on antibody partner, with a larger interface area in 1C1m-Fc antibody complexes. Furthermore, these complexes seem to be more stable and with lower RMSF. The mutation produces an additional positive influence on the binding by increasing the number of H-bonds between the 1C1m-Fc antibody with both the human and murine TEM1 subtypes. Future investigations focused on all the specific residues involved in the interface changes are foreseen. Such structural approach, taking into account all the protein-protein interactions (PPIs), was however out of the scope of the present work.

4. Conclusions

Taken together, our results have allowed us to identify a promising candidate, 1C1m-Fc, as a suitable targeting molecule for the development of TEM1-targeted radioimmunoconjugates. The *in vitro* and *in vivo* biological performance of the radioiodinated 1C1m-Fc fragment compares favourably with observations reported for other antibody fragments used in more advanced pre-clinical studies. The *in silico* approach provided useful rationale and insight into our experimental results and may represent a valuable tool to achieve improved antibody-antigen interactions in the future. We believe that the 1C1m-Fc clone merits further investigation of its utility for theranostic applications, both following radioiodination with suitable medical iodine radioisotopes and, in addition, with other relevant radionuclides.

5. Materials and methods

5.1. Antibody production

The 1C1 and 1C1m scFv clones were sub-cloned into a pTT-based mammalian expression vector [43]. The vector was engineered to contain a downstream and in-frame hinge and the human IgG1 CH2CH3 constant domains, to allow the production of scFv-Fc fusion proteins. Recombinant proteins were produced using the mammalian HEK293-6E/pTT transient expression system (National Research Council of Canada; obtained under licence). HEK293-6E cells were grown in Freestyle F17 medium (Thermo Fisher Scientific, #A13835) containing 4 mM GlutaMAX (Life Technologies, #35050061), 0.1% Pluronic® F-68 (Life Technologies, #24040032) and 25 μg/mL G418 (Life Technologies, #10131019) at 37 °C, 5% CO2 and 120 rpm. For transfection, the vector DNA was mixed with FectoPRO (Polyplus, #116-010) transfection reagent in F17 medium without supplements, according to the manufacturer's instructions. After five days of culture to allow protein expression, cultures were subjected to low speed centrifugation and the media collected. Samples could be used immediately for direct capture and immobilization (dCI) experiments or snap-frozen and stored at −80 °C until required. ScFv-Fc fusions were purified from clarified expression media using a HiTrap™ MabSelect column (GE Healthcare, #11003494), followed by extensive dialysis against phosphate-buffered saline (PBS) [30].

5.2. ^{125}I radiolabelling

5.2.1. IODOGEN

The radiolabelling was performed according to the IODOGEN method [34]. Briefly, aliquots of antibody fragments (58–70 μg) in PBS

were transferred into vials pre-coated with 100 μg of IODOGEN (Sigma Aldrich). The appropriate amount of $Na^{125}I$ (Perkin Elmer), with activities ranging from 5 to 50 MBq, was then added to the mixture and left reacting during 5 min at room temperature. The antibodies were then purified from unreacted residual ^{125}I by ultrafiltration using Amicon filters with 10 kDa cut-off, and recovered in PBS.

5.2.2. Bolton Hunter

The radiolabelling was performed with slight modifications to the Bolton-Hunter procedure [35]. A small volume of the radioiodinated Bolton-Hunter reagent (Perkin Elmer) was transferred to an Eppendorf vial and the THF evaporated under a nitrogen flux before the addition of approximately 35 μg of 1C1m-Fc antibody in 0.1 M Borate Buffer at pH 8.5. After 15 min of reaction at 0 °C, the ^{125}I-1C1m-Fc antibody was purified from unreacted residual ^{125}I and other labelled products by ultrafiltration using Amicon filters with 10 kDa cut-off. After purification, ^{125}I-1C1m-Fc was recovered in PBS.

5.3. Determination of the radiochemical purity

5.3.1. ITLC

After ultrafiltration, the antibodies were obtained with a radiochemical purity up to 99% as determined by radio-TLC using ITLC-SG strips eluted with MeOH/H_2O (7:3) and by detection of the radioactivity in the strips on a miniGITA scanning device (Elysia Raytest). The data were analyzed using the Gina analysis software (Elysia Raytest) after manual integration of the peaks. In this system, the radiolabelled antibodies remain at $R_f = 0$ while the unbound ^{125}I radiochemical species migrate to the solvent front.

5.3.2. HPLC

Size Exclusion-HPLC analyses were performed on a PerkinElmer Flexar UHPLC System (PerkinElmer) coupled to the Gabi Nova γ-detector (Elysia-raytest, Angleur, Belgium). Compounds were separated using a Waters XBridgeTM Protein BEH SEC column (300 × 7.8 mm, 200 Å pore size, 3.5 μm particle size, 0.7 mL/min flow rate). Isocratic elution was performed using 0.1 M phosphate buffer pH 6.5 as mobile phase. Elution was monitored via absorbance at 220/280 nm or γ detection.

5.4. Radiochemical stability

The antibodies were diluted in at least four times the volume of PBS at pH 7.2 or cell culture media and incubated over 48 h at 37 °C and 4 °C. At the selected time points, a drop of the radioactive solution was placed on an ITLC strips and eluted with MeOH/H_2O (7:3). The strips were measured on a miniGITA scanning device and the results analysed after manual integration of the peaks using Gina software (Elysia Raytest).

5.5. Data analysis and statistics

All curve-fitting and statistical analyses were conducted using Prism 7.0 software (GraphPad). For Fig. 8 b the statistical significance was determined by multiple t-tests (one per row) using the Holm-Sidak method, with alpha = 0.05 and each row was analyzed individually, without assuming a consistent SD. For Fig. 10 the statistical significance was determined by multiple t-tests (one per row) using the Holm-Sidak method, with alpha = 0.05 where each row was analyzed individually, without assuming a consistent SD.

5.6. Gel electrophoresis experiments

Analysis by Sodium Dodecyl Sulphate - PolyAcrylamide Gel Electrophoresis (SDS-PAGE) of native and radioiodinated scFv-Fcs was performed under reducing and non-reducing conditions. For SDS-Page in non-reducing conditions an equal volume of non-reducing sample buffer (31.25 mM Tris (pH 6.8), 1.5% (w/v) SDS, 10% (v/v) glycerol, 0.001% (w/v) bromophenol blue) was added to each sample and the mixture stirred. Samples of approximately 10 μg were loaded per lane and resolved in a 10% polyacrylamide gel in a Mini-PROTEAN Tetra Cell apparatus (Biorad, USA). Electrophoresis proceeded at 120 V during 2 h in running buffer (0.025 M Tris, 0.192 M glycine, 0.1% (w/v) SDS). Proteins bands were visualized by staining gels with Bio-Safe Coomassie Blue G-250 stain (BioRad) and destained by washing with water for 30 min. Molecular weight standards (Color Burst Electrophoresis Markers, Sigma-Aldrich, St. Louis, MO, USA) were also loaded in the gels for reference. Finally, gels were placed between two cellophane sheets and dried in vacuum and heat for long term storage.

5.7. Determination of the immunoreactive fraction (IRF)

The immunoreactive fraction (IRF) of ^{125}I-1C1m-Fc was assessed by a conventional saturation assay, extrapolated to infinite antigen by a rectangular hyperbola. A high-binding 96- well microplate (Costar #3590, Corning) was coated with decreasing amount of recombinant human TEM1 protein (LS-G85947-20, LSBio, Seattle, WA, USA) in phosphate buffered saline (PBS) (100 μL, from 100 to 1.56 nM) for 16 h at 4 °C. After flicking the plate and washing three times with PBS (200 μL), the wells were blocked for 2 h with blocking buffer (2% BSA, 1 μM EDTA and 0.05% Tween-20 in PBS). Three empty wells were also blocked for nonspecific binding determination. The wells were rinsed with PBS before the addition of a solution of ^{125}I-1C1m-Fc in blocking buffer (100 μL, 0.18 nM). The same volume of ^{125}I-1C1m-Fc solution was also pipetted in three γ-counter tubes as an internal control for the measurement of the total activity and in the three empty wells that were previously blocked for a blank triplicate (U_{Blank}). The plate was incubated for 16 h at 4 °C. The supernatant was collected in γ-counter tubes, the wells rinsed once on ice with cold PBS and the pooled liquid was counted in a calibrated gamma-counter (Wallac Wizard, Perkin Elmer). The specific binding (B_{Spec}) was calculated for each dilution step as the difference in counts between the mean unbound supernatant of the blank ($\overline{U}_{Blank}$) and the unbound supernatant $(U) : B_{Spec} = \overline{U}_{Blank} - U$. A hyperbolic fit extrapolation of $B/T = B_{Spec}/\overline{U}_{Blank}$ at infinite antigen concentration was done using Graphpad Prism 7 to provide the IRF value. An assumption was made of a single binding site per antigen. The mathematical aspect of this method was fully validated in a separate publication [38].

5.8. In vitro studies

5.8.1. Cell culture

Two endosialin/TEM1-positive tumor cell lines, human A673 (ATCC CRL-1598) and murine 2H11 (ATCC CRL-2163) and one endosialin/TEM1 negative murine cell line, MS1 (ATCC CRL-2279) were used for *in vitro* assays. The cells were maintained in Dulbecco's modified Eagle's medium (DMEM) with GlutaMAX and supplemented with 10% fetal bovine serum (FBS). All cells were maintained at 37 °C, 5% CO_2 in a humidified incubator and the absence of mycoplasma from all cell lines was confirmed by regular testing.

5.8.2. Cellular uptake assays

The cells were plated in quadruplicate in 24-wells cell culture plates at a concentration of 2.5×10^5 cells/well in 500 μL of complete culture media. The following day, the medium was removed and the adherent cells incubated with approximately 20 KBq (0.5–0.7 μCi) of ^{125}I labelled scFv-Fc antibodies in 500 μL fresh media (humidified atmosphere with 5% CO_2 at 37 °C). At each of the six time points (30 min, 1 h, 2 h, 4 h, 19 h and 24 h), the medium was removed and the cells washed twice with cold PBS at pH 7.2. Cells were then lysed with 1 M NaOH and the lysates transferred to tubes and measured in a gamma counter to assess cell associated activity. The results were expressed as percentage of bound

activity per million cells.

5.8.3. Blocking assays

Blocking studies were performed similarly to cellular uptake assays. The cells were plated in quadruplicate in 24-wells cell culture plates at a concentration of 2.5 × 10^5 cells/well in 500 μL of complete culture media. The following day, the medium was removed and the adherent cells incubated with approximately 20 KBq (0.5–0.7 μCi) of ^{125}I labelled scFv-Fc antibodies and 6 μg of cold antibody to saturate the specific binding sites. The radiolabelled and cold antibodies were added using solutions in complete culture media and wells had a final volume of 500 μL.

5.8.4. Internalization assays

Cellular internalization assays were performed in quadruplicate in 24-wells cell culture plates at 2,5 × 10^5 cells/well in 500 μL of complete culture media and incubated at 37 °C for a period of 24 h. The following day, the medium was removed and the adherent cells incubated with ^{125}I-radiolabelled scFv-Fc antibodies and left in humidified atmosphere with 5% CO_2 at 37 °C. At each of the six time points (30 min, 1 h, 2 h, 4 h, 19 h and 24 h), the cells were washed with ice-cold medium to stop the incubation. Cell-surface-bound radioactivity was removed by two steps of acid wash using 50 mM HCl-Glycine buffer at pH 2.7 during 5 min at room temperature. The pH was neutralized with cold PBS with 0.2% BSA, and subsequently the cells were lysed by 5 min incubation with 1 M NaOH at 37 °C to determine internalized radioactivity. The radioactivity associated to each fraction was measured in a gamma counter and the internalized fraction expressed as the percentage of total added activity per 10^6 cells.

5.8.5. Saturation assays

Cells were incubated in triplicate at 4 °C during 4 h with increasing concentrations of the ^{125}I-radiolabelled scFv-Fc antibodies (0.1 nM–25 nM) plus a nonspecific binding control sample containing cold antibody (approx. 2 μM). After the incubation, the radioactive solution was removed, and the cells washed with fresh PBS. Successively, NaOH 1 M was added and the rest of cell suspension was transferred into test tubes for measurement in a gamma counter. Analysis of the results by non-linear regression using GraphPad Prism 7, allowed determination of the ligand binding affinity K_d and the maximum number of binding sites B_{max}.

5.9. Biodistribution studies

Animal studies were conducted in conformity with the national law and with the EU Guidelines for Animal Care and Ethics in Animal Experimentation. The animals were housed in a temperature- and humidity-controlled room with a 12 h light/12 h dark schedule and with access to water and food ad libitum. Biodistribution of the ^{125}I-1C1m-Fc antibody, radiolabelled following the Iodogen procedure, was evaluated in 10–12 weeks old NMRI-Nude female mice (Charles River) with A673 xenografts, weighing approximately 18–22 g. A 70 μL bolus containing a suspension of 5 × 10^6 freshly harvested human A673 cells in Matrigel was subcutaneously injected in the right shoulder of each mouse. The animals were kept under aseptic conditions and 14 days later developed tumours with an average size of 124 ± 35 mm^3 at the inoculation site. Two days before injection of the ^{125}I-1C1m-Fc, KI (1 mg/mL) and $KClO_4$ (2 mg/mL) were added to the water bottle to limit thyroid uptake of free Iodine-125. Xenograft-bearing animals were intravenously injected by tail vein administration of ^{125}I-1C1m-Fc (9 kBq, 0.2 μg of 1C1m-Fc) diluted in 100 μL of NaCl 0.9%. The animals were co-injected with 10 mg/kg of IgG to saturate neonatal Fc receptor. At 4, 24, 48 and 72 h, tissues of interest were dissected, weighed, and their radioactivity was measured using a γ-counter (Wizard 1470 Gamma Counter, PerkinElmer). The uptake of ^{125}I-1C1m-Fc in the tissues was calculated and expressed as the average of the percentage of the injected radioactivity dose per gram of tissue (n = 3 or 2 for every time point).

5.10. In silico studies

5.10.1. Model construction and molecular docking

The 3D structures of hu/muTEM1 fragments (87% sequence identity) within 324–390 region were constructed by homology modelling using the MODELLER package, and the protein template P07204 (PDBID: 1DX5L) [44–46]. The structures obtained were clustered and the lowest 20 free-energy conformations were identified. I-TASSER was used to model the three-dimensional structure of the 1C1-Fc antibody fragment [47]. There are several approaches to validate homology models such as built-in metrics of open-source and licensed software. In our study, we chose the combination of MODELLER's metrics, ProSA-web and ProQ to provide a reliable protocol to create valid models to be used in the molecular docking studies [48–50]. The 1C1m-Fc THR233ILE mutation was performed using Pymol wizard [51]. Docking was performed with the HADDOCK2.2 web server [52]. Default parameters were used, and the modelled 1C1 scFv-Fc and 1C1m scFv-Fc that interact with TEM1 was selected for docking. The resulting docked orientations within a RMSD of 2 Å were clustered together. The interface for each complex was determined using PyMOL v2.0 with the Interface Residues python script, which employs a cutoff value for the difference in the solvent-accessible areas of each protein to determine interface residues. Using a cutoff value of 5, PyMOL predicted the 1C1-Fc and 1C1m-Fc portion of the Fc/TEM interface. The highest HADDOCK scores complexes were then used for the MD simulations studies.

5.10.2. Molecular dynamics simulations

MD simulations of huTEM1/1C1-Fc, huTEM1/1C1m-Fc, muTEM1/1C1-Fc and muTEM1/1C1m-Fc were performed using GROMACS 2018.3 and the Amber ff99SB-ILDN force field [53–56]. Each complex was solvated by a TIP3P water box with 12 Å buffering distance to the boundary, which was verified throughout the simulations. The simulation systems were kept neutral by adding the necessary counterions. Simulations were performed in the NPT (isothermal-isobaric) ensemble. Temperature coupling was performed using the v-rescale thermostat at 300 K, with a coupling constant of 0.1 ps, while an isotropic Parrinello-Rahman barostat was used to keep the pressure constant at 1 bar using a coupling constant of 2.0 ps and a compressibility of 4.5 × 10^{-5} bar^{-1} [57–59]. The initial system energy was first minimised for 50.000 steps, followed by two equilibrations of 250 ps. Three production runs were performed for each system, each 100 ns-long. The RMSF calculations were carried out in GROMACS version 2018.3 [53–55].

5.10.3. Protein-protein interfacial characterization

In-house Visual-Molecular-Dynamics (VMD) script were used to calculate H-Bonds between residues in the interfaces [60]. Interfacial residues were defined as any residues where C-alphas were within a 5 Å cut-off of the other chain to ensure that no meaningful interaction was lost due to loop movement during MD. Pymol script was used to define these interfaces.

Declaration of Competing Interest

The authors declare that they have no known competing financial interests or personal relationships that could have appeared to influence the work reported in this paper.

Acknowledgements

This research project has been supported by a Marie Skłodowska-Curie Innovative Training Network Fellowship of the European Commission's Horizon 2020 Programme under contract number 642889 MEDICIS-PROMED. This work was also supported by Fundação para a Ciência e Tecnologia (project UID/Multi/04349/2019) and by the

Alfred and Annemarie von Sick Swiss-Card-Onco Grant (Zurich, Switzerland).

Appendix A. Supplementary data

Supplementary data to this article can be found online at https://doi.org/10.1016/j.ejpb.2020.11.015.

References

[1] R.M. Sharkey, D.M. Goldenberg, Cancer radioimmunotherapy, Immunotherapy 3 (2011) 349–370, https://doi.org/10.2217/imt.10.114.

[2] C.D. Martins, G. Kramer-Marek, W.J.G. Oyen, Radioimmunotherapy for delivery of cytotoxic radioisotopes: current status and challenges, Expert Opin. Drug Deliv. 15 (2018) 185–196, https://doi.org/10.1080/17425247.2018.1378180.

[3] S.M. Larson, J.A. Carrasquillo, N.K.V. Cheung, O.W. Press, Radioimmunotherapy of human tumours, Nat. Rev. Cancer 15 (2015) 347–360, https://doi.org/10.1038/nrc3925.

[4] H. Zhou, X. Fu, Q. Li, T. Niu, Safety and efficacy of anti-PD-1 monoclonal antibodies in patients with relapsed or refractory lymphoma: a meta-analysis of prospective clinic trails, Front. Pharmacol. 10 (2019), https://doi.org/10.3389/fphar.2019.00387.

[5] M. Eskian, M.H. Khorasanizadeh, P.L. Zinzani, T.M. Illidge, N. Rezaei, Novel methods to improve the efficiency of radioimmunotherapy for non-hodgkin lymphoma, Int. Rev. Immunol. 38 (2019) 79–91, https://doi.org/10.1080/08830185.2019.1588266.

[6] K. Hohloch, Radioimmunotherapy of lymphoma: an underestimated therapy option, Lancet Haematol. 4 (2017) e6–e7, https://doi.org/10.1016/S2352-3026(16)30188-0.

[7] C. Bodet-Milin, F. Kraeber-Bodéré, T. Eugène, F. Guérard, J. Gaschet, C. Bailly, M. Mougin, M. Bourgeois, A. Faivre-Chauvet, M. Chérel, P. Chevallier, Radioimmunotherapy for treatment of acute leukemia, Semin. Nucl. Med. 46 (2016) 135–146, https://doi.org/10.1053/j.semnuclmed.2015.10.007.

[8] M.D. Bartholomä, Radioimmunotherapy of solid tumors: approaches on the verge of clinical application, J. Label. Compd. Radiopharm. 61 (2018) 715–726, https://doi.org/10.1002/jlcr.3619.

[9] E.D.G. Fleuren, Y.M.H. Versleijen-Jonkers, S. Heskamp, C.M.L. van Herpen, W.J. G. Oyen, W.T.A. van der Graaf, O.C. Boerman, Theranostic applications of antibodies in oncology, Mol. Oncol. 8 (2014) 799–812, https://doi.org/10.1016/j.molonc.2014.03.010.

[10] A.L. Nelson, Antibody fragments: hope and hype, MAbs. 2 (2010) 77–83, https://doi.org/10.4161/mabs.2.1.10786.

[11] A. Bates, C.A. Power, David vs. Goliath: The Structure, Function, and Clinical Prospects of Antibody Fragments, Antibodies. 8 (2019) 28. https://doi.org/10.3390/antib8020028.

[12] B.A. Teicher, CD248 : A therapeutic target in cancer and fibrotic diseases, 10 (2019) 993–1009.

[13] S. Christian, H. Ahorn, A. Koehler, F. Eisenhaber, H.P. Rodi, P. Garin-Chesa, J. E. Park, W.J. Rettig, M.C. Lenter, Molecular cloning and characterization of endosialin, a C-type lectin-like cell surface receptor of tumor endothelium, J. Biol. Chem. 276 (2001) 7408–7414, https://doi.org/10.1074/jbc.M009604200.

[14] C. Rouleau, D.A. Gianolio, R. Smale, S.D. Roth, R. Krumbholz, J. Harper, K. J. Munroe, T.L. Green, B.C. Horten, S.M. Schmid, B.A. Teicher, Anti-endosialin antibody-drug conjugate: potential in sarcoma and other malignancies, Mol. Cancer Ther. 14 (2015) 2081–2089, https://doi.org/10.1158/1535-7163.MCT-15-0312.

[15] E. Capone, E. Piccolo, I. Fichera, P. Ciufici, D. Barcaroli, A. Sala, V. De Laurenzi, V. Iacobelli, S. Iacobelli, G. Sala, Generation of a novel Antibody-Drug Conjugate targeting endosialin: potent and durable antitumor response in sarcoma, Oncotarget 8 (2017) 60368–60377. https://doi.org/10.18632/oncotarget.19499.

[16] A. Zhao, S. Nunez-Cruz, C. Li, G. Coukos, D.L. Siegel, N. Scholler, Rapid isolation of high-affinity human antibodies against the tumor vascular marker Endosialin/TEM1, using a paired yeast-display/secretory scFv library platform, J. Immunol. Methods. 363 (2011) 221–232, https://doi.org/10.1016/j.jim.2010.09.001.

[17] S. Ugel, J.G. Facciponte, F. De Sanctis, A. Facciabene, Targeting tumor vasculature: expanding the potential of DNA cancer vaccines, Cancer Immunol. Immunother. 64 (2015) 1339–1348, https://doi.org/10.1007/s00262-015-1747-8.

[18] S. Christian, R. Winkler, I. Helfrich, A.M. Boos, E. Besemfelder, D. Schadendorf, H. G. Augustin, Endosialin (Tem1) Is a Marker of Tumor-Associated Myofibroblasts and Tumor Vessel-Associated Mural Cells, 172 (2008) 486–494. https://doi.org/10.2353/ajpath.2008.070623.

[19] R. Becker, M.C. Lenter, T. Vollkommer, A.M. Boos, D. Pfaff, H.G. Augustin, S. Christian, Tumor stroma marker endosialin (Tem1) is a binding partner of metastasis-related protein Mac-2 BP/90K, FASEB J. 22 (2008) 3059–3067, https://doi.org/10.1096/fj.07-101386.

[20] B. Tomkowicz, K. Rybinski, B. Foley, W. Ebel, B. Kline, E. Routhier, P. Sass, N.C. Nicolaides, L. Grasso, Y. Zhou, Interaction of endosialin / TEM1 with extracellular matrix proteins mediates cell adhesion and migration SCIENCES, (2007) 1–6.

[21] E.B. Carson-Walter, B.N. Winans, M.C. Whiteman, Y. Liu, S. Jarvela, H. Haapasalo, B.M. Tyler, D.L. Huso, M.D. Johnson, K.A. Walter, Characterization of TEM1/endosialin in human and murine brain tumors, BMC Cancer 9 (2009) 1–13, https://doi.org/10.1186/1471-2407-9-417.

[22] A. Nanda, B. Karim, Z. Peng, G. Liu, W. Qiu, C. Gan, B. Vogelstein, B.S. Croix, K. W. Kinzler, D.L. Huso, Tumor endothelial marker 1 (Tem1) functions in the growth and progression of abdominal tumors, Proc. Natl. Acad. Sci. U. S. A. 103 (2006) 3351–3356, https://doi.org/10.1073/pnas.0511306103.

[23] Y. Guo, J. Hu, Y. Wang, X. Peng, J. Min, J. Wang, E. Matthaiou, Y. Cheng, K. Sun, X. Tong, Y. Fan, P.J. Zhang, L.E. Kandalaft, M. Irving, G. Coukos, C. Li, Tumour endothelial marker 1/endosialin-mediated targeting of human sarcoma, Eur. J. Cancer. 90 (2018) 111–121, https://doi.org/10.1016/j.ejca.2017.10.035.

[24] L.A. Diaz, C.M. Coughlin, S.C. Weil, J. Fishel, M.M. Gounder, S. Lawrence, N. Azad, D.J. O'Shannessy, L. Grasso, J. Wustner, W. Ebel, R.D. Carvajal, A first-in-human phase i study of MORAb-004, a monoclonal antibody to endosialin in patients with advanced solid tumors, Clin. Cancer Res. 21 (2015) 1281–1288, https://doi.org/10.1158/1078-0432.CCR-14-1829.

[25] R.E. Norris, E. Fox, J.M. Reid, A. Ralya, X.W. Liu, C. Minard, B.J. Weigel, Phase 1 trial of ontuxizumab (MORAb-004) in children with relapsed or refractory solid tumors: a report from the Children's Oncology Group Phase 1 Pilot Consortium (ADVL1213), Pediatr. Blood Cancer. 65 (2018) 1–8, https://doi.org/10.1002/pbc.26944.

[26] A.-M. Chacko, C. Li, M. Nayak, J.L. Mikitsh, J. Hu, C. Hou, L. Grasso, N. C. Nicolaides, V.R. Muzykantov, C.R. Divgi, G. Coukos, Development of 124I immuno-PET targeting tumor vascular TEM1/endosialin, J. Nucl. Med. 55 (2014) 500–507, https://doi.org/10.2967/jnumed.113.121905.

[27] C. Li, J. Wang, J. Hu, Y. Feng, K. Hasegawa, X. Peng, X. Duan, A. Zhao, J.L. Mikitsh, V.R. Muzykantov, A.M. Chacko, D.A. Pryma, S.M. Dunn, G. Coukos, Development, optimization, and validation of novel anti-TEM1/CD248 affinity agent for optical imaging in cancer, Oncotarget 5 (2014) 6994–7012. https://doi.org/10.18632/oncotarget.2188.

[28] F. Cicone, T. Denoël, S. Gnesin, N. Riggi, M. Irving, G. Jakka, N. Schaefer, D. Viertl, G. Coukos, J.O. Prior, Preclinical evaluation and dosimetry of [111In]CHX-DTPA-scFv78-Fc Targeting Endosialin/Tumor Endothelial Marker 1 (TEM1), Mol. Imaging Biol. (2020), https://doi.org/10.1007/s11307-020-01479-8.

[29] F. Cicone, S. Gnesin, T. Denoël, T. Stora, N.P. van der Meulen, C. Müller, C. Vermeulen, M. Benešová, U. Köster, K. Johnston, E. Amato, L. Auditore, G. Coukos, M. Stabin, N. Schaefer, D. Viertl, J.O. Prior, Internal radiation dosimetry of a 152Tb-labeled antibody in tumor-bearing mice, EJNMMI Res. 9 (2019), https://doi.org/10.1186/s13550-019-0524-7.

[30] J.K. Fierle, J. Abram-Saliba, M. Brioschi, M. deTiani, G. Coukos, S.M. Dunn, Integrating SpyCatcher/SpyTag covalent fusion technology into phage display workflows for rapid antibody discovery, Sci. Rep. 9 (2019) 1–15, https://doi.org/10.1038/s41598-019-49233-7.

[31] B.A. Teicher, R.G. Bagley, C. Rouleau, A. Kruger, Y. Ren, L. Kurtzberg, Characteristics of human Ewing/PNET sarcoma models, Ann. Saudi Med. 31 (2011) 174–182, https://doi.org/10.4103/0256-4947.78206.

[32] A. Martínez-Ramírez, S. Rodríguez-Perales, B. Meléndez, B. Martínez-Delgado, M. Urioste, J.C. Cigudosa, J. Benítez, Characterization of the A673 cell line (Ewing tumor) by molecular cytogenetic techniques, Cancer Genet. Cytogenet. 141 (2003) 138–142, https://doi.org/10.1016/s0165-4608(02)00670-2.

[33] J. Walter-Yohrling, S. Morgenbesser, C. Rouleau, R. Bagley, M. Callahan, W. Weber, B.A. Teicher, Murine endothelial cell lines as models of tumor endothelial cells, Clin. Cancer Res. 10 (2004) 2179–2189, https://doi.org/10.1158/1078-0432.CCR-03-1013.

[34] G.S. Bailey, The Iodogen Method for Radiolabeling Protein, Protein Protoc. Handb. 5 (1996) 673–674, https://doi.org/10.1007/978-1-60327-259-9_115.

[35] A.E. Bolton, W.M. Hunter, The labelling of proteins to high specific radioactivities by conjugation to a 125I containing acylating agent. Application to the radioimmunoassay, Biochem. J. 133 (1973) 529–538, https://doi.org/10.1042/bj1330529.

[36] G.G. Bornstein, Antibody drug conjugates: preclinical considerations, AAPS J. 17 (2015) 525–534, https://doi.org/10.1208/s12248-015-9738-4.

[37] A. Lucas, L. Price, A. Schorzman, M. Storrie, J. Piscitelli, J. Razo, W. Zamboni, Factors affecting the pharmacology of antibody-drug conjugates, Antibodies 7 (2018) 10, https://doi.org/10.3390/antib7010010.

[38] T. Denoël, L. Pedrelli, G. Pantaleo, J.O. Prior, A robust method for assaying the immunoreactive fraction in nonequilibrium systems, Pharmaceuticals 12 (2019), https://doi.org/10.3390/ph12040177.

[39] C. Li, A.M. Chacko, J. Hu, K. Hasegawa, J. Swails, L. Grasso, W.S. El-Deiry, N. Nicolaides, V.R. Muzykantov, C.R. Divgi, G. Coukos, Antibody-based tumor vascular theranostics targeting endosialin/TEM1 in a new mouse tumor vascular model, Cancer Biol. Ther. 15 (2014) 443–451, https://doi.org/10.4161/cbt.27825.

[40] X. Yuan, M. Yang, X. Chen, X. Zhang, S. Sukhadia, N. Musolino, H. Bao, T. Chen, C. Xu, Q. Wang, S. Santoro, D. Ricklin, J. Hu, R. Lin, W. Yang, Z. Li, W. Qin, A. Zhao, N. Scholler, G. Coukos, Correction to: Characterization of the first fully human anti-TEM1 scFv in models of solid tumor imaging and immunotoxin-based therapy (Cancer Immunology, Immunotherapy, (2017), 66, 3, (367-378), 10.1007/s00262-016-1937-z), Cancer Immunol. Immunother. 67 (2018) 329–339. https://doi.org/10.1007/s00262-017-2101-0.

[41] S.J. de Vries, M. van Dijk, A.M.J.J. Bonvin, The HADDOCK web server for data-driven biomolecular docking, Nat. Protoc. 5 (2010) 883–897, https://doi.org/10.1038/nprot.2010.32.

[42] V.E. Schneeberger, V. Allaj, E.E. Gardner, J.T. Poirier, C.M. Rudin, Quantitation of murine stroma and selective purification of the human tumor component of patient-derived xenografts for genomic analysis, PLoS One 11 (2016) 1–16, https://doi.org/10.1371/journal.pone.0160587.

[43] Y. Durocher, S. Perret, A. Kamen, High-level and high-throughput recombinant protein production by transient transfection of suspension-growing human 293-

EBNA1 cells, Nucleic Acids Res. 30 (2002) E9. https://www.ncbi.nlm.nih.gov/pubmed/11788735.
[44] X. Yuan, M. Yang, X. Chen, X. Zhang, S. Sukhadia, N. Musolino, Characterization of the first fully human anti - TEM1 scFv in models of solid tumor imaging and immunotoxin - based therapy, Cancer Immunol. Immunother. (2016), https://doi.org/10.1007/s00262-016-1937-z.
[45] U. Pieper, B.M. Webb, D.T. Barkan, D. Schneidman-Duhovny, A. Schlessinger, H. Braberg, Z. Yang, E.C. Meng, E.F. Pettersen, C.C. Huang, R.S. Datta, P. Sampathkumar, M.S. Madhusudhan, K. Sjölander, T.E. Ferrin, S.K. Burley, A. Sali, ModBase, a database of annotated comparative protein structure models, and associated resources, Nucleic Acids Res. 39 (2011) 465–474, https://doi.org/10.1093/nar/gkq1091.
[46] P. Fuentes-Prior, Y. Iwanaga, R. Huber, R. Paglia, G. Rumennik, M. Seto, J. Morser, D.R. Light, W. Bode, Structural basis for the anticoagulant activity of the thrombin-thrombomodulin complex, Nature 404 (2000) 518–525, https://doi.org/10.1038/35006683.
[47] A. Roy, A. Kucukural, Y. Zhang, I-TASSER: a unified platform for automated protein structure and function prediction, Nat. Protoc. 5 (2010) 725–738, https://doi.org/10.1038/nprot.2010.5.
[48] B. Webb, A. Sali, Comparative protein structure modeling using MODELLER, Curr. Protoc. Bioinforma. 54 (2016) 139–148, https://doi.org/10.1002/cpbi.3.
[49] M. Wiederstein, M.J. Sippl, ProSA-web: Interactive web service for the recognition of errors in three-dimensional structures of proteins, Nucleic Acids Res. 35 (2007) 407–410, https://doi.org/10.1093/nar/gkm290.
[50] B. Wallner, A. Elofsson, Can correct protein models be identified? Protein Sci. 12 (2003) 1073–1086, https://doi.org/10.1110/ps.0236803.
[51] W.L. DeLano, Pymol: an open-source molecular graphics tool, CCP4 Newsl, Protein Crystallogr. 40 (2002) 82–92.
[52] G.C.P. Van Zundert, J.P.G.L.M. Rodrigues, M. Trellet, C. Schmitz, P.L. Kastritis, E. Karaca, A.S.J. Melquiond, M. Van Dijk, S.J. De Vries, A.M.J.J. Bonvin, The HADDOCK2.2 Web Server: user-friendly integrative modeling of biomolecular complexes, J. Mol. Biol. 428 (2016) 720–725, https://doi.org/10.1016/j.jmb.2015.09.014.
[53] H.J.C. Berendsen, D. van der Spoel, R. van Drunen, GROMACS: a message-passing parallel molecular dynamics implementation, Comput. Phys. Commun. 91 (1995) 43–56, https://doi.org/10.1016/0010-4655(95)00042-E.
[54] D. Van Der Spoel, E. Lindahl, B. Hess, G. Groenhof, A.E. Mark, H.J.C. Berendsen, GROMACS: fast, flexible, and free, J. Comput. Chem. 26 (2005) 1701–1718, https://doi.org/10.1002/jcc.20291.
[55] M.J. Abraham, T. Murtola, R. Schulz, S. Páll, J.C. Smith, B. Hess, E. Lindah, Gromacs: high performance molecular simulations through multi-level parallelism from laptops to supercomputers, SoftwareX 1–2 (2015) 19–25, https://doi.org/10.1016/j.softx.2015.06.001.
[56] K. Lindorff-Larsen, S. Piana, K. Palmo, P. Maragakis, J.L. Klepeis, R.O. Dror, D. E. Shaw, Improved side-chain torsion potentials for the Amber ff99SB protein force field, Proteins Struct. Funct. Bioinforma. 78 (2010) 1950–1958, https://doi.org/10.1002/prot.22711.
[57] G. Bussi, D. Donadio, M. Parrinello, Canonical sampling through velocity rescaling, J. Chem. Phys. 126 (2007) 14101, https://doi.org/10.1063/1.2408420.
[58] S. Nosé, M.L. Klein, Constant pressure molecular dynamics for molecular systems, Mol. Phys. 50 (1983) 1055–1076, https://doi.org/10.1080/00268978300102851.
[59] M. Parrinello, A. Rahman, Polymorphic transitions in single crystals: a new molecular dynamics method, J. Appl. Phys. 52 (1981) 7182–7190, https://doi.org/10.1063/1.328693.
[60] W. Humphrey, A. Dalke, K. Schulten, VMD: visual molecular dynamics, J. Mol. Graph. 14 (1996) 33–38, https://doi.org/10.1016/0263-7855(96)00018-5.